Heliyon 10 (2024) e30360

Contents lists available at ScienceDirect

Heliyon

journal homepage: www.cell.com/heliyon

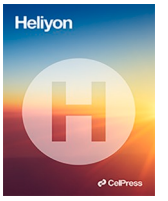

Research article

Adult aberrant astrocytes submitted to late passage cultivation lost differentiation markers and decreased their pro-inflammatory profile

Gabriel Otero [a,1], Carmen Bolatto [b,a,1], Eugenia Isasi [a,b], Sofía Cerri [a], Paola Rodríguez [a], Daniela Boragno [a], Marta Marco [a,c], Cristina Parada [b], Matías Stancov [a], María Noel Cuitinho [a], Silvia Olivera-Bravo [a,*]

[a] Department of Neurobiology and Neuropathology (NBNP), Instituto de Investigaciones Biológicas Clemente Estable (IIBCE), Montevideo, Uruguay
[b] Department of Histology and Embryology, Facultad de Medicina, Universidad de la República (UdelaR), Montevideo, Uruguay
[c] Department of Clinical Biochemistry, School of Chemistry (UdelaR), Montevideo, Uruguay

ARTICLE INFO

Keywords:
Aberrant glial cells
Permanent lack of homeostatic properties
Non-cell autonomous disease
Microenvironment-dependent inflammation properties

ABSTRACT

In amyotrophic lateral sclerosis (ALS), astrocytes are considered key players in some non-cell non-neuronal autonomous mechanisms that underlie motor neuron death. However, it is unknown how much of these deleterious features were permanently acquired. To assess this point, we evaluated if the most remarkable features of neurotoxic aberrant glial phenotypes (AbAs) isolated from paralytic rats of the ALS model G93A Cu/Zn superoxide dismutase 1 (SOD1) could remain upon long lasting cultivation. Real time PCR, immunolabelling and zymography analysis showed that upon many passages, AbAs preserved the cell proliferation capacity, mitochondrial function and response to different compounds that inhibit some key astrocyte functions but decreased the expression of parameters associated to cell lineage, homeostasis and inflammation. As these results are contrary to the sustained inflammatory status observed along disease progression in SOD1G93A rats, we propose that the most AbAs remarkable features related to homeostasis and neurotoxicity were not permanently acquired and might depend on the signaling coming from the injuring microenvironment present in the degenerating spinal cord of terminal rats.

1. Introduction

Amyotrophic lateral sclerosis (ALS) is a neurodegenerative disease characterized by progressive loss of upper and lower motor neurons, increasing inflammation and reactive gliosis [1,2], all leading to muscle atrophy, progressive paralysis, and death between 3 and 5 years post-diagnosis. ALS has a predominant sporadic etiology, but up to 10 % of the cases are familial [2,3], with 15 % of them linked to mutations in the enzyme Cu/Zn superoxide dismutase 1 (SOD1) [4,5]. Interestingly, when some of the dominant SOD1

* Corresponding author.
E-mail addresses: gotero@fcien.edu.uy (G. Otero), cbolatto@fmed.edu.uy (C. Bolatto), eugeniaisasi@fmed.edu.uy (E. Isasi), scerrifassio@gmail.com (S. Cerri), paokr26@gmail.com (P. Rodríguez), danielaboragno@gmail.com (D. Boragno), mmarco@fq.edu.uy (M. Marco), cristinap123@gmail.com (C. Parada), mstancov14@gmail.com (M. Stancov), marianoelcuitinho@gmail.com (M.N. Cuitinho), solivera2011@gmail.com (S. Olivera-Bravo).
[1] Both authors contributed equally.

https://doi.org/10.1016/j.heliyon.2024.e30360
Received 15 August 2023; Received in revised form 15 April 2024; Accepted 24 April 2024
Available online 26 April 2024

mutations found in ALS patients were expressed in rodent motor neurons and astrocytes or microglia [10], an age-related motor syndrome that mimics many of the pathological features of the human disease was elicited [2,6–9,11–13]. Thus, implying that motor neurons and glia participate in most of the pathological mechanisms and damaging events described in these ALS murine models [2,14–17]. Moreover, it has been reported that astrocytes, either those bearing the human mutated isoform SOD1G93A [18–20] or those obtained from ALS patients, could kill motor neurons [21–23], suggesting a prominent role of astrocytes in disease pathogenesis.

Existing evidence about the active role of astrocytes during motor neuron death in ALS models was reinforced with the isolation of a novel type of aberrant astrocytes -named as AbAs- that appear in the spinal cord (SC) of symptomatic SOD1G93A (Tg) rats and were exceptionally toxic to motor neurons [24]. These cells present distinctive ultrastructural features and highly remarkable pathological signs not found in normal astrocytes [24,25], including the absence of replicative senescence and the ability to survive to numerous passages [24], both highly relevant in the neuron-glia defective communication [26,27] that seems to underlie neurodegeneration. Accordingly, it has been shown that focal transplantation of AbAs into the lumbar SC of wild type rats caused extensive gliosis and motor neuron damage a week after the injection [28]. At this time, injected cells remained intermingled between reactive glia and ubiquitinated motor neurons, suggesting that they may boost neuroinflammation and spread motor neuron damage [28]. In accordance, AbAs were isolated either from the lumbar SC of Tg rats with paralytic legs or from the cervical SC when the paralysis initiated in the forepaws [29], all suggesting that AbAs may emerge as a local response to motor neuron damage and further spread along the SC during disease progression [29].

However, it is still unknown how much of the AbAs′ features were permanently acquired or can change along culturing. To assess this point, we analyzed the mRNA and protein levels of some of the major players involved in astrocyte homeostatic [30,31] or inflammatory [32–35] properties in AbAs **at** low (LP, 6–8) vs. high (HP, 16–18) passages. Concerning homeostatic functions, glial glutamate transporter 1 (GLT1), glutamine synthase (GS) and S100β protein were analyzed. GLT1 and GS were selected because they are the main effectors in the glutamate/glutamine cycle by determining the glutamate uptake from the synaptic cleft [30,31] and by catalyzing its conversion to the glutamine that will be used by neurons. Interestingly, the glutamate/glutamine cycle also regulates nitrogen metabolism and ammonia levels, determining the synthesis of the step-limiting glutathione precursors [26,36,37], and linking the most important homeostatic functions that protect against excitotoxicity and oxidative stress. In fact, it has been proposed that decreased GLT1 expression is enough to elicit excitotoxicity [30,31], and that changes in GS expression or activity could significantly contribute to the pathogenesis of several neurological disorders including ALS [38]. The calcium binding protein S100β was analyzed because it is proposed as a danger-associated molecular pattern that triggers the activation of the transcription factor Nuclear Factor Kappa B Subunit 1 (NF-κB) and downstream increased expression and release of pro-inflammatory cytokines, and also because it is associated to disturbed cell proliferation [39,40]. Status of endoplasmic reticulum (ER) stress and mitochondrial functionality were assessed in LP and HP AbAs, mostly because of the key astrocyte metabolic support to neurons [36] that is disturbed at many levels upon damaging conditions. To further know if changes in AbAs′ features along culturing influence their survival upon exposure to different pharmacological challenges, LP and HP AbAs were submitted to several compounds that damage homeostatic astrocytes [24,41–44] or either offer neuroprotection in the SOD1G93A model from which the AbAs were obtained [45].

In addition, as astrocytes are considered key regulators of inflammation with time and context-dependent responses [2,18,46,47], including the exacerbation of inflammatory processes by releasing pro-inflammatory cytokines during reactivity [36,39,40], we have analyzed interleukin-1β (IL-1β) and tumor necrosis factor-α (TNF-α) in AbAs′ conditioned medium. IL-1β was analyzed because glial IL-1β was proposed as a causative event of neuroinflammation and as one of the first altered signals in ALS [48]. We also were focused on TNF-α because it is an important component of the neuroinflammatory response and it may inhibit glutamate transport on astrocytes [49]. Thus, it could link neuroinflammation and excitotoxicity, two preponderant pathological mechanisms occurring in ALS as well as in several neurodegenerative diseases.

We were also interested in evaluating the activity of matrix metalloproteinases 2 and 9 (MMP-2 and -9) in AbAs′ conditioned medium because these proteases are considered as fine tuners of neuroinflammation [32–35]. Both enzymes, as all MMPs, are zinc-dependent proteases capable of degrading several substrates, including basal membranes and extracellular matrix components [32–35]. Both enzymes are synthesized and secreted as latent/inactive forms that are further activated within the extracellular medium by other active MMPs or by serine proteinases. Under physiological conditions, MMPs′ actions are tightly balanced by their inhibitors [33], but MMPs/MMP inhibitor imbalance play a role in various central nervous system (CNS) disorders, including ALS [33–35]. In this regard, it has been described that exacerbated MMP-2 and -9 levels contribute to neuroinflammation by activating inflammation-potentiating pathways, either directly (i.e. by converting the membrane-bound TNF-α into the soluble, active form [33]), or indirectly by activating the enzymes that further will process the signaling molecules related to inflammation [33,34]. MMP-2 and -9 may also play themselves as neuroinflammatory signals capable of triggering glial activation and consequent secretion of pro-inflammatory cytokines [33,34]. Both may also control the extracellular pools of pro-inflammatory cytokines and chemokines, either via the release of surface bound forms as mentioned for TNF-α or by enzymatic degradation as described for IL-1β due to MMP-2 activity [33,48]. In turn, TNF-α may stimulate MMP-2 and -9 transcription reinforcing neuroinflammation through an auto-amplifying deleterious loop [49]. In the context of ALS, MMP-2 and -9 increased their expression along ALS progression in many disease models and patient samples [32,34,35]. In addition, MMP-9 had been proposed as a determinant of selective motor neuron vulnerability, because it was found highly expressed in damaged dying motor neurons [33].

The analysis of the markers evaluated on AbAs was done in the SC tissue from non transgenic (NoTg) and Tg asymptomatic and symptomatic/terminal rats at 120 and 200-210 day-old, because SC samples from symptomatic Tg animals are the tissue source from which AbAs were isolated. Levels of these markers were compared with those shown in asymptomatic Tg and in age-matched NoTg animals. The summary of obtained results indicates that AbAs′ continued proliferating along the passages but lost their main features associated with the astrocyte lineage and their pro-inflammatory profile.

2. Materials and methods

All cell culture materials were purchased from Gibco (MA, USA). General chemicals came from Sigma (MO, USA); primary antibodies were bought from Sigma, abcam (MA, USA), Cell Signaling (MA, USA), Thermo Fisher Scientific (MA, USA) or Peprotech (NJ, USA). The BrdU antibody came from DAKO (CA, USA). Primers were from Macrogen (Seoul, Korea), and materials for qPCR came from Qiagen (MD, USA). Secondary antibodies were Thermo Fisher Scientific. Violacein was kindly provided by Dr. S. Castro-Sowinski (School of Sciences, UdelaR, Uruguay) and purified by Dr. D. Davyt group (School of Chemistry UdelaR, Uruguay) and Dr. D. Alem (IIBCE, Uruguay).

2.1. Animals

Male hemizygous rats NTac: SD-TgN (SOD1G93A) L26H (Taconic, NY, USA), originally developed by Howland et al. (2002) [8], were grown at the IIBCE animal house as outbred Sprague-Dawley background with food and water ad libitum and controlled environmental conditions (12 h dark/light cycle; 21 ± 3 °C). Harems were made with one hemizygous Tg male and two wild type Sprague Dawley female rats of 90 day-old. Genotyping was performed as previously described in Vargas et al. (2006), immediately after weaning [50]. Age-matched NoTg animals were used as controls. All procedures (including animal processing and primary culture protocols) were approved by the Institutional Ethical Committee for the Use of Animals with Research Purposes (CEUA-IIBCE, Protocol Number 004/09/2015). Such Committee integrates the National Commission for Animal Experimentation (CNEA) that follows the 18611 National Law for the Use of Animals in Experimentation, Teaching and Scientific Research, and the "Guide for the Care and Use of Laboratory Animals: Eight Edition" of the National Institutes of Health (USA).

To make AbAs cultures, seven independent cultures were made using seven symptomatic/terminal Tg rats of 200–210 day-old with both lower limbs paralyzed. Cultures from Tg rats were replicated up to passage 20 and experiments were done in sequential passages 6, 7 and 8 (low passages) and at 16, 17 and 18 passages (high passages). Five NoTg rats were used in primary cultures of adult astrocytes to compare some parameters with LP AbAs because primary astrocytes do not survive to many passages [24,25].

To obtain SC homogenates or sections, we employed seven asymptomatic (120 day-old) and seven symptomatic/terminal (200-210 day-old) Tg animals together with the same number of NoTg age-matched animals. Those ages were selected because at 120 day-old, body weight and gait of Tg rats are indistinguishable from those of age-matched NoTg brothers. Instead, at 210 day-old, Tg animals are in a definite symptomatic/terminal stage, with both legs completely paralyzed, lost more than 50 % of their body weight and their mobility clearly altered causing a hard access to food and water, both offered ad libitum. The onset of the symptomatic stage was determined when the body weight started to drop or when the clinical examination (three times a week) detected the presence of an abnormal gait that is typically evidenced as subtle limping or dragging of one hind limb. The animal colony employed in this work had an onset of the symptomatic stage (~180 day-old) and lifespan (~200-210 day-old) significantly delayed when compared with the original report [8], but is entirely on the dates indicated by the supplier (Taconic).

2.2. Cell cultures and preparation for analysis

Procedures employed were described by Diaz-Amarilla et al. (2011) [24] with minor modifications. Briefly, animals were deeply anesthetized with 90:10 mg/kg ketamine:xylazine and decapitated. Then, the lumbar SC cord was quickly dissected, cleaned, chopped and dissociated with 0.5 % trypsin-EDTA during 25 min at 37 °C in a water bath. Trypsin was inhibited with DMEM-HEPES containing 10 % fetal bovine serum (FBS). Tissue disaggregation was achieved by repeated pipetting; the cell suspension was passed through an 80 μm mesh to eliminate tissue debris and spun 10 min at 200 g. The pellet obtained was re-suspended in culture medium (DMEM-HEPES-$NaHCO_3$ + 10 % FBS + 100 IU/ml penicillin +100 μg/mL streptomycin) and then was plated in a 25 cm^2 tissue culture flask. Culture medium was removed after 24 h and then replaced every 48 h until confluence. Then, cells were passaged every week after repeated trypsinization in the same conditions explained above. In all cases, 1×10^6 cells in 5 ml of culture medium were seeded per 25 cm^2 culture flask. After confluence, each flask yielded up to 2.5×10^6 cells that were divided and expanded in two 25 cm^2 bottles until used. Lumbar SC cultures from NoTg animals yielded few cells that resisted only two/three passages. Passages analyzed were obtained from successive splitting during passages 6 to 8 (LP) and 16 to 18 (HP), lasting in culture until confluence.

To prepare LP and HP cell samples for qPCR, media culture was completely retired, 1 ml of Trizol reagent was added and homogenized samples immediately frozen at −80 °C [50].

To obtain conditioned media to be used in gelatin zymography and dot blot analysis, confluent primary astrocytes from adult NoTg rats, LP and HP cells were cultured in DMEM-HEPES without FBS during 48 h. After that, media was collected, spun during 10 min at 500 g to retire cell debris [51] and immediately frozen at −80 °C until use.

To immunostain cells, five-seven independent sets of LP and HP cultures were washed with 10 mmol/L, pH 7.4 phosphate buffered saline solution (PBS), fixed with 4 % paraformaldehyde (PFA) during 20 min, washed 3 times with PBS and submitted to immunocytochemistry assays.

2.3. Analytical approaches made in LP and HP AbAs

2.3.1. Immunocytochemistry [51,52,55,60]

Fixed LP and HP AbAs were permeabilized with 0.1 % Triton X-100 during 30 min, washed 3 times with PBS and blocked 30 min with 5 % bovine serum albumin (BSA). Then cells were incubated with one or two of the following antibodies: 1:500 anti-GLT1 (Cell

Signaling, #3838); 1:600 anti-S100β (Sigma, S2532); 1:500 anti-GS (abcam, 49873); 1:300 anti-MMP-2 (Thermo Fisher Scientific, 436000), 1:500 anti-MMP-9 (Thermo Fisher Scientific, PA5-13199) or 1:300 anti-78-kDa glucose-regulated protein (GRP78/BiP, abcam, ab-21685). After a 4 °C overnight incubation and 3 washes with PBS, cells were incubated for 90 min with 1:800 dilutions of 1 mg/mL secondary antibodies conjugated to Alexa fluorescent probes (Thermo Fisher Scientific). Then cells were washed and mounted in 50 % glycerol containing 1 μg/mL 4′, 6-diamino-2-phenylindole (DAPI). As negative controls, the primary or secondary antibodies were omitted. A part of the cells were labeled with 1:500 Phalloidin-FITC (Thermo Fisher Scientific, *F*432), rinsed 2 times with PBS and mounted in glycerol/DAPI. All of the cells were imaged between 24 h and 48 h after the labeling procedure was completed.

2.3.2. Cell proliferation determination

Three independent batches of LP and HP cells were exposed to 5-bromo-2′-deoxyuridine (BrdU, 10 μmol/L) during 24 h [52]. After that, cells were washed 3 times with PBS, fixed with 4 % PFA, permeabilized with 0.3 % Triton X-100 and DNA denatured with 2 N HCl during 45 min. After several washes, cells were incubated overnight with 1:500 of anti-BrdU antibody (DAKO, M0744) in 0.3 % Triton X-100 buffered solution. Then washes and incubation with secondary antibody were done as indicated above (immunocytochemistry, 2.3). Rate of cell proliferation was determined as percent of BrdU + cells/DAPI + cells. Values were represented as percent of proliferation rate of LP AbAs.

2.3.3. Pharmacological treatments and cell viability determination

Once confluence was reached in AbAs from LP and HP passages, media was changed to DMEM+2 % FBS to ensure quiescence. The day after, cultures were treated during 24 h with 10 μmol/L Forskolin (FSK) [44], 2.5 μmol/L Tunicamycin (TN) [43], 100 μmol/L Zinc chloride (Zn) [42] or 300 μmol/L 6-aminonicotinamide (6AN) [41]. In another set of experiments, LP and HP AbAs were submitted to vehicle (0.1 % DMSO) or 150 and 300 nmol/L violacein, respectively [29,45]. Determination of cell viability was made with the sulforhodamine B (SRB) method [53] according to manufacturer instructions. Briefly, ¼ of cell culture medium of 50 % trichloroacetic acid was added to each well of 96 multiwell plates seeded with 2×10^4 cells per cm^2. After 1 h at 4 °C, the liquid volume was completely discarded and adherent cells washed 5x with distilled water. Wells were left drying 2 days in darkness at room temperature, and then incubated 30 min with 0.4 % SRB in 1 % acetic acid. After 5x washes with 1 % acetic acid, cells were dried in darkness. The next day, 100 μL of 10 mmol/L, pH 10 Tris base was added to each well, agitated until complete dissolution and read at 490 and 690 nm in a Varioskan spectrophotometer. Specific optical absorbance (490–690 nm) was determined for each experimental condition and represented as box plots with min and max values of all independent experiments performed. Data were related to the survival of LP AbAs in control condition.

2.3.4. Determination of mitochondrial activity

The 3-(4,5-dimethylthiazol-2-yl)-2,5-diphenyltetrazolium bromide (MTT) assay based on activity of NAD(P)H oxidoreductases [54] was employed as an approach to assess AbAs mitochondrial functionality as previously demonstrated in astrocytes [52]. To do this, astrocytes, LP and HP AbAs were seeded in 96 multiwell plates during 5 days. Then, half of the plate was incubated with 1 μg/ml Hoechst 33342 and the other half with 0.1 mg/ml MTT during 45 min at 37 °C. After that, whole volume was retired from each well, and 100 μL PBS added to wells incubated with Hoechst 33342 or 100 μL DMSO with those treated with MTT. Then, the absolute absorbance (MTT) or fluorescence (Hoechst 33342) were measured in a Varioskan spectrophotometer at 405 nm for Hoechst 33342 and 570 and 630 nm for MTT, respectively. Data from MTT was related to that of Hoechst 33342 values shown in the same experimental conditions to avoid the influence of different numbers of cells. Results were related to the MMT/Hoechst 33342 ratio of LP AbAs.

2.4. Processing of animals

2.4.1. Samples for qPCR, zymography and dot blotting

At the age established, rats were quickly decapitated with a guillotine and the body immediately immersed in ice. Lumbar SC was dissected and half of the tissue was collected in 500 μL Trizol and immediately frozen at −80 °C until processed for qPCR analysis. The other half was collected in tissue lysis buffer (100 ml of 10 mmol/L, pH = 7.4, PBS containing 4 mM EDTA and a tablet of SIGMA-FAST™ protease inhibitors) and immediately frozen at −80 °C until used in zymography or in dot blotting assays.

2.4.2. Animal fixation and SC dissection for immunohistochemistry

Ketamine: xylazine anesthetized animals were submitted to transcardial perfusion with 0.9 % saline and 4 % PFA in 10 mmol/L, pH 7.4 PBS, at a constant flow of 1 mL/min [54]. Fixed SC was removed, post-fixed by immersion in 4 % PFA during 24 h at 4 °C, and then 30 μm transverse sections were serially obtained on a vibrating microtome. Then, free-floating sections were washed 3 times with 10 mmol/L, pH 7.4 PBS (5 min each), and submitted to the immunolabeling protocol described in immunocytochemistry (2.3.1). A batch of SC sections of each age from NoTg and Tg animals was incubated with 1:500 anti-IL-1β antibody (500-P21BG, Peprotech) and immunolabeling done using the same protocol.

2.5. Methodological approaches made in AbAs' cultures and SC samples

2.5.1. RNA extraction and cDNA synthesis

Total RNA was extracted using Trizol™ reagent (Invitrogen) following the manufacturer's instructions. To eliminate genomic DNA

contamination, RNA samples were treated with DNase-free™ kit (Applied Biosystem) and then quantified using a NanoDrop spectrophotometer (Thermo Scientific). Each reverse transcription consisted of 1–1.4 μg of total RNA, Oligo (dT) primers, Enzyme Mix and carried out with the RETROscript™ kit (Ambion) according to the manufacturer's instructions.

2.5.2. Quantitative real-time PCR (qPCR)

Real time PCR reactions were performed using the SYBR™ Green PCR Kit (QuantiNovaTM, Qiagen). Each qPCR reaction contained 0.5 ng of cDNA (template), 1x of SYBR™ Green Master Mix and 0.4 μM of each gene-specific primer. Primer sequences were as follows: β-act: 5′-CAGCCTTCCTTCCTGGGTAT-3' (forward), 5′-CTGTGTTGGCATAGAGGTCTT-3' (reverse); GS: 5′-CCACTGTCCCTGGGCTTAGTTTA-3' (forward), 5′-AGTGACATGCTAGTCCCACCAA (reverse); GLT-1: 5′-AGGAGCCAAAGCACCGAAAC-3' (forward), 5′-CCCGGGAAGGCTATCAACAT-3' (reverse); and S100β: 5′-TGCCCTCATTGATGTCTTCCA-3' (forward), 5′-GAGAGAGCTCGTTGTTGATGAGCT-3' (reverse). The final volume was adjusted to 10 μL with nuclease-free water. The real-time PCR program employed was: an activation step at 95 °C for 2 min, followed by 40 cycles at 95 °C for 10 s and 60 °C for 30 s, and performed using the Rotor-Gene 6000™ (Corbett Research). The amplifications were performed in triplicates with a negative control in each run. Specificity of PCR amplifications was monitored with melting curve analysis using the Rotor-Gene Q series software. The relative expression of each target gene was analyzed with the 2-(delta delta CT) (2-ΔΔCT) method [56] using β-actin as the reference gene [57,58]. The averaged data obtained for each gene in LP cells were considered as 1, and those of HP related to this value.

2.5.3. Zymography

Frozen samples at −80 °C were defrosted and maintained in ice, sonicated with 3 pulses of 30 s each and spun at 12000 g, during 10 min at 4 °C. Protein concentration was determined by the bicinchoninic acid procedure with minor modifications [24,50]. Then, 20 μg protein of each condition was analyzed by gelatin zymography, according to Marco et al. (2020) [59]. Briefly, 0.1 % cell culture grade gelatin was copolymerized into 1-mm-thick 8 % polyacrylamide gel and each sample loaded as well as MMP-2 and MMP-9 recombinant enzymes as positive controls. BSA was employed as the negative control. Each gel was electrophoresed at 100 V, washed 2 times with 2.5 % Triton X-100, rinsed 3 times in distilled water, and incubated for 18 h at 37 °C in 50 mmol/L, pH 7.6 Tris buffer containing 5 mmol/L $CaCl_2$, 20 mmol/L NaCl and 0.005 % Brij 35. After that, each gel was stained with 1 % Coomassie Brilliant Blue R-250 and then destained until the appearance of white zones evidencing gelatin degradation. The area of each white band was determined with FIJI-Image J (NIH, USA) and expressed as absolute units (AU) related to total proteins (g).

2.5.4. Dot blotting assays

Dot blots were the approach selected to determine presence of IL-1β and TNF-α in AbAs conditioned medium as well as in SC homogenates according to Olivera-Bravo et al., 2022 [45]. Briefly, 2 μL of each sample, containing the same amount of protein, was slowly spotted on a piece of nitrocellulose membrane. Once the membrane was dried, non-specific binding was blocked with 5 % BSA in TBS-0.05 % Tween 20 (TBS-T, 1 h, room temperature) and then incubated with 1:1000 anti-IL-1β (ab234437, abcam or 500-P21BG, Peprotech) or anti-TNF-α (ab 234437, abcam or 500-P31A, Peprotech) in 0.1% BSA:TBST or 1:2500 anti-β actin (A5316, Sigma). After 30 min at room temperature, 3 washes were done with TBST-T. Incubation with 1:2000 anti-mouse or anti-rabbit secondary antibodies conjugated with HRP was done during 30 min, washed 3 times with TBS-T and a final wash with TBS. Membrane was incubated with ECL (Thermo Fisher, 34577) and then read in an iBright FL1500 Imaging System. The net integrated density for all of the conditions was measured in FIJI-Image J.

2.6. Image acquisition

Fluorescent probes and immunofluorescence were imaged in an upright FV300 Olympus confocal microscope provided with 405, 488, 546, and 633 nm lasers. 2048 × 2048 microphotographs of 5–7 representative areas of each culture were taken with all acquisition parameters identical for LP and HP cells or SC sections. Once pictures were obtained, DAPI + cells were counted. To assess signal intensity, the mean gray value (MGV, intensity per number of pixels) was measured with FIJI/ImageJ. A signal was considered positive when it at least doubled the background. Normalized fluorescence was determined by subtracting the MGV of the background to the value determined inside the positive signal.

2.7. Data analysis and statistical studies

Data was obtained upon analyzing the results of seven independent experiments using cells at passages 6, 7, and 8, each one by triplicate or quintuplicate, in each experiment of LP condition. The same procedure was done with cells at 16, 17 and 18 passages for HP analysis, respectively. The data of each experiment was pooled to obtain the averaged value together with the standard deviation per experiment.

For the sake of comparison, as primary cultured astrocytes from NoTg animals do not survive up to high passages and experience replicative senescence [62], most of the data represented in this work was related to values found in LP AbAs (taken as 100 % or 1 in gene expression analysis). Each chart was done using GraphPad Prism 8.3, and the represented box plots contain the minimal and maximal values obtained after pooling all the independent experiments.

Statistical analysis was performed using GraphPad Prism 8.3. Descriptive statistics were used for each group. The comparison between LP vs. HP pairs was made with unpaired Student *t*-test when normality was passed. Comparison between different SC sample groups was done with ordinary one-way ANOVA with Tukey test for multiple comparisons. Otherwise, non-parametric tests were

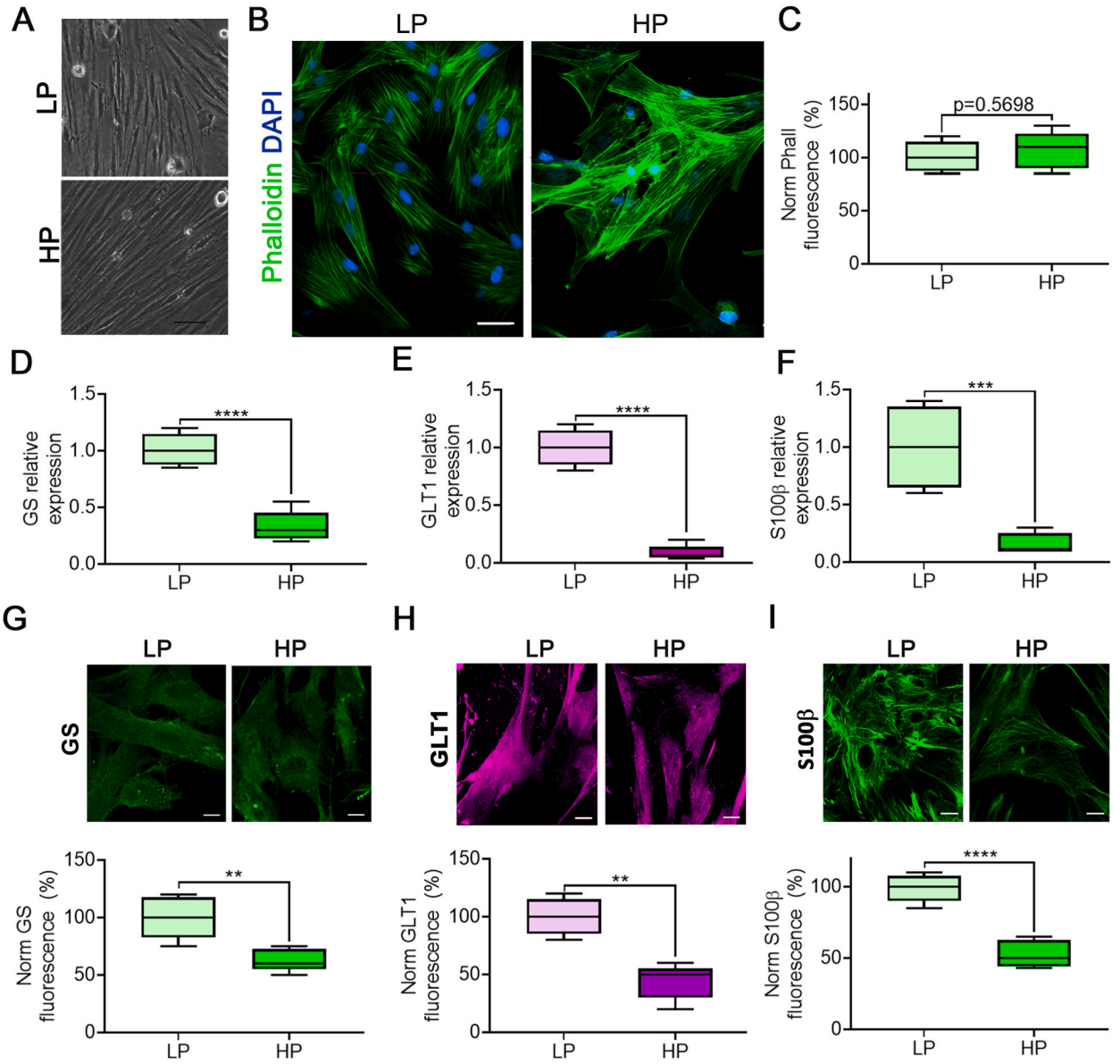

Fig. 1. Expression of astrocyte markers in LP and HP AbAs. (**A**) Representative light microscopy images of low density cultures at low (LP) and high (HP) passages evidencing a predominant elongated shape (Magnification: 10 ×). (**B**) Phalloidin-fluorescein labelling showing the preservation of actin cytoskeleton and very similar morphology when comparing HP vs. LP cultures. Note the tendency of HP cells to grow in multilayers even with available cell free areas. Calibration bars: 50 μm. (**C**) Normalized Phalloidin fluorescence was measured as specific mean gray value (MGV, positive signals minus the background), and showed no differences in HP vs. LP cells (150 cells per replica, 3 replicas per condition, 7 independent experiments). For this and all graphs, the values for LP cells were represented in light colors while those for HP cells are represented in more intense colors. (**D**–**F**) Statistically significant decreases in gene expression of GS (**D**), GLT1 (**E**) and S100β (**F**) in HP vs. LP cultures assessed by qPCR. Values represented in HP cells as fold of the averaged data obtained for each gene in LP cells (5 replicates per passage, 7 independent experiments including all the passages). (**G**–**I**) Immunocytochemistry against GS (**G**), GLT1 (**H**) and S100β (**I**) denoting the same tendency of the results found with qPCR. Calibration bars: 50 μm. Below each pair of images there is the quantitative analysis of each respective MGV (150 cells per replica, 3 replicas per condition, 7 independent experiments). The data of each experiment was pooled as one value. The box charts show the minimal and maximal values obtained after representing the averaged value of all independent experiments. In all the charts associated with fluorescent images cases, LP conditions were taken as 100 %. For this, and all figures, the asterisks represent $p < 0.05$ (*), $p < 0.01$ (**), $p < 0.001$ (***) and $p < 0.0001$ (****), respectively. n.s. indicates non-significant statistical difference. (For interpretation of the references to color in this figure legend, the reader is referred to the Web version of this article.)

applied. A value of $p < 0.05$ was considered statistically significant.

3. Results

3.1. Comparison of HP vs. LP AbAs: what remains and what changes upon long lasting cultivation

● Preserved morphology along culturing

Upon the initial culture stages, at the passages analyzed, AbAs maintained their appearance along culturing as seen in light microscopy images that show elongated cells growing close to each other as well as scarce intermingled bright rounded proliferating cells (Fig. 1A). After the labeling with the Alexa 488-Phalloidin probe that binds actin filaments (F-actin), is was also evidenced a similar arrangement of F-actin stress fibers in LP and HP AbAs in spite of the HP increased cell density and overlapping (Fig. 1B). Intensity of the Alexa 488-Phalloidin signal expressed as specific MGV (positive signal minus background) showed no significant differences between HP vs. LP cultures ($p = 0.5698$) (Fig. 1C).

● Decreased gene expression and immunofluorescence of typical astrocyte markers

When comparing HP vs. LP AbAs by qPCR, results showed statistically significant decreases (↓) in the expression of the three genes analyzed as follows: GS ~ ↓ 67 % ($p < 0.0001$) (Fig. 1D); GLT1 ~ ↓ 94 % ($p < 0.0001$) (Fig. 1E), and S100β ~ ↓ 84 % ($p < 0.0009$) (Fig. 1F). Immunoreactivity against these three proteins also showed decreased levels along passages with GS ~ ↓ 77 % ($p = 0.0041$) (Fig. 1G); GLT1 ~ ↓ 56 % ($p = 0.0004$) (Fig. 1H), and S100β ~ ↓ 47 % ($p < 0.0001$) (Fig. 1I). Remarkably, when comparing LP AbAs with NoTg astrocytes, differences in the immunoreactivity were decreases in GS (~↓ 30 %, $p = 0.0008$) and in GLT1 (~↓ 75 %, $p < 0.0001$) but significant increases (↑) in S100β (~↑ 250 %, $p < 0.0001$), respectively. These results were similar to that previously

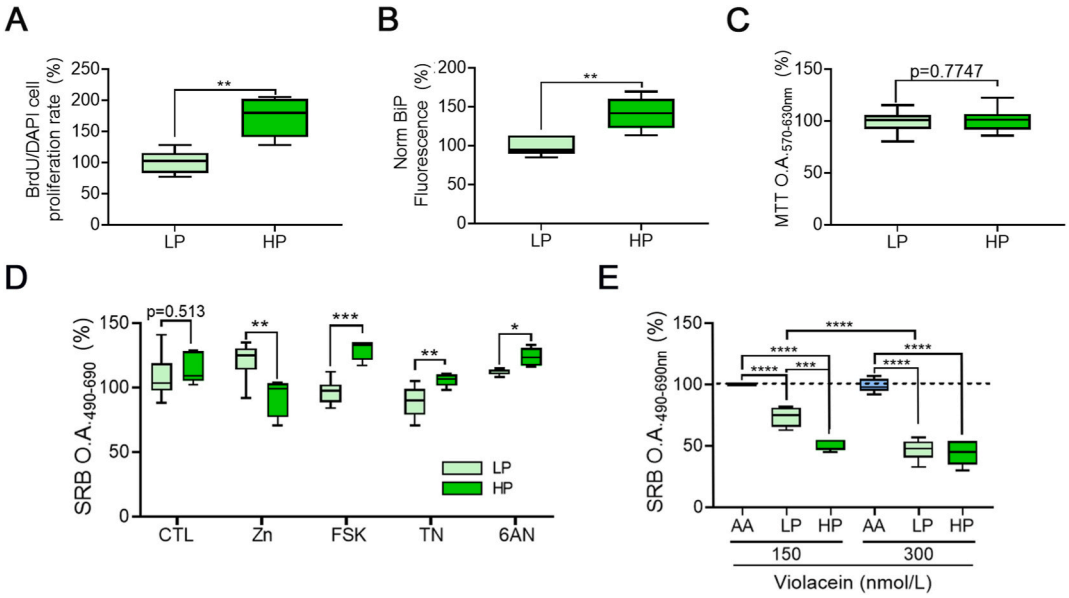

Fig. 2. Functional parameters and pharmacological response upon long lasting cultivation. (**A**) Increased proliferation rate in HP vs. LP cultures assessed with BrdU immunolabeling and determined as the percentage of BrdU positive cells related to total DAPI positive cells (150 cells per replica, 3 replicas per condition, 3 independent experiments). Values represented were related to proliferation rate of LP cells (100 %). (**B**) Significantly augmented ER stress in HP vs. LP cells evaluated by GRP78/BiP immunostaining (150 cells per replica, 3 replicas per condition, 3 independent experiments). Data found in LP cells were assigned as 100 %. (**C**) Preserved mitochondrial functionality in HP vs. LP cultures assessed by MTT assay. Results obtained indicate absence of changes when comparing LP vs. HP averaged values (5 replicas per passage, 7 independent experiments). (**D**) Effects of 100 μmol/L Zinc chloride (Zn), 10 μmol/L Forskolin (FSK), 2.5 μmol/L Tunicamycin (TN) and 300 μmol/L 6-aminonicotinamide (6AN) on LP and HP cells′ survival assessed with the sulforhodamine B (SRB) method. Except for Zn, SRB values increased in HP vs. LP cultures indicating more living instead of deadly cells (5 replicas per condition and passage, 7 independent experiments). (**E**) Selective vulnerability of AbAs to violacein in comparison to primary astrocytes from adult NoTg animals (AA). Results obtained indicate that LP and HP AbAs′ showed differences in viability at 150 nmol/L violacein; and that the viability of LP, but not of HP AbAs, decreased upon the exposure to 150 and 300 nmol/L violacein (5 replicates of AA, LP and HP per condition, 7 independent experiments). The 100 % value in the y-axis (dashed line) correspond to the viability obtained in AA in control conditions. Values represented in min to max box plots were obtained after pooling the data of each experiment (taken as a single value) and calculating the averaged value of all independent experiments. Data from LP cells were represented in pale green colors whereas those of HP cells are in more intense green, and those from AA appear in blue. (For interpretation of the references to color in this figure legend, the reader is referred to the Web version of this article.)

reported in Diaz-Amarilla et al. (2011) [24] suggesting that cells obtained in this work were very similar to the founding paper and that this deleterious phenotype could be consistently obtained from paralytic SOD1G93A rats.

- Increased cell proliferation and ER stress

HP vs. LP AbAs showed increased cell proliferation rate (~↑ 73 %, $p = 0.0024$) (Fig. 2A) and ER stress (~↑ 42 %, $p = 0.0054$) assessed by immunoreactivity against GRP78/BiP [25] (Fig. 2B). Instead, MTT results showed similar mitochondrial activity measured as the performance of the NAD(P)H dehydrogenases, with small non-significant differences among both groups (~2 %, $p = 0.7747$) (Fig. 2C). When comparing to NoTg astrocytes (not shown), LP AbAs in basal conditions showed a cell proliferation four times higher (~↑ 300 %, $p < 0.0001$) and GRP78/BiP signal that was more than fivefold times bigger (~↑ 430 %, $p < 0.0001$), respectively.

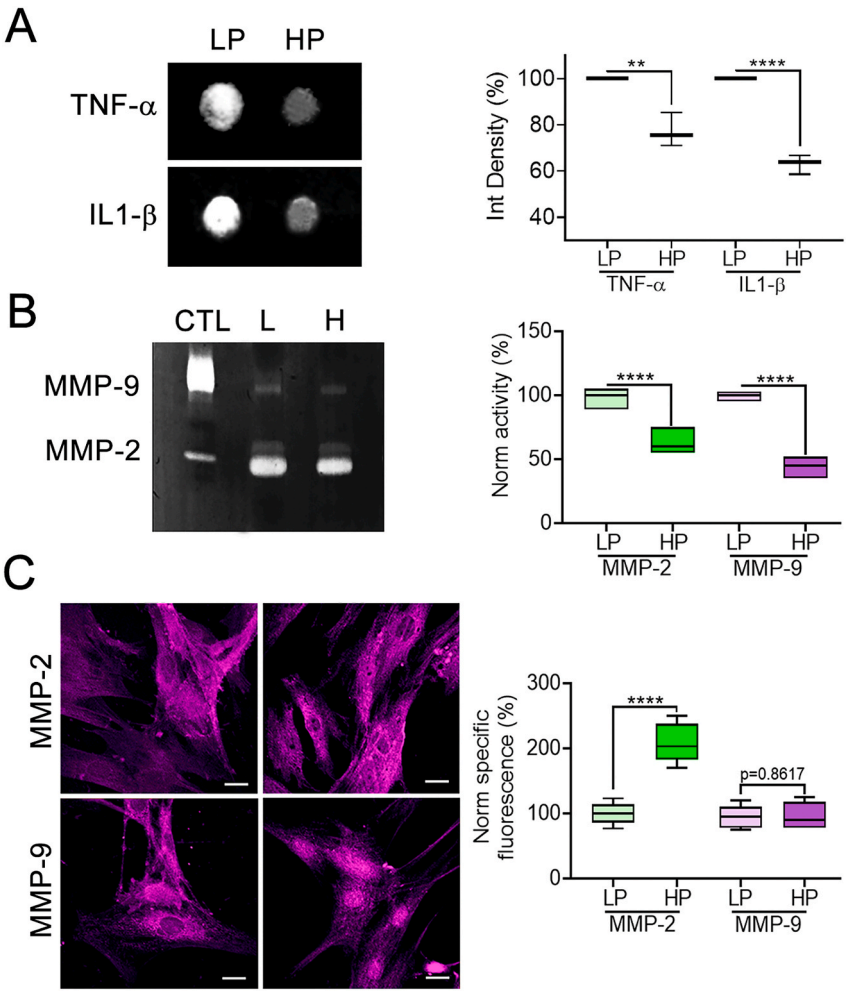

Fig. 3. Inflammation markers and MMPs in AbAs. (A) Dot blot on the left showing the positive signals for TNF-α and IL-1β in LP and HP conditioned medium. Note the significant decreased signals in HP cells (5 replicates per passage, 7 independent experiments including all the passages). The chart on the right shows the integrated density of each spot taking LP as 100 %. Each value was previously related to the integrated density of β-actin taken as the loading control. BSA was used as a negative control. Recombinant TNF-α was employed as the positive control. **(B)** A gel zymogram showing white bands that evidence gelatin degradation due to MMP-9 and MMP-2 activities in LP AbAs but decreased MMP-2 and almost complete disappearance of MMP-9 activity in HP cells. The left lane is a positive control **(CTL)** made with equal amounts of recombinant MMP-2 and MMP-9 proteins. The chart on the right shows the quantitation of band areas and the statistical significance of differences determined upon HP vs. LP comparison (5 replicates per passage, 7 independent experiments including all the passages). In the charts, LP values were represented in pale green and fuchsia, and HP data appear in intense colors. **(C)** MMP-2 and MMP-9 immunoreactivity in LP and HP AbAs showing specific cytoplasmic signals. The right chart shows the quantitative analysis evidencing increased specific fluorescence (MGV with the background subtracted) in MMP-2 and unchanged MMP-9 signals in HP vs. LP AbAs (150 cells per replica, 3 replicas per condition, 7 independent experiments). Results from LP cells were represented in pale colors whereas those of HP cells appear more intense colored. Data from MMP-2 were represented in green and from MMP-9 in fuchsia. Complete dot blots and zymograms of Fig. 3A and B are in Supplementary material. (For interpretation of the references to color in this figure legend, the reader is referred to the Web version of this article.)

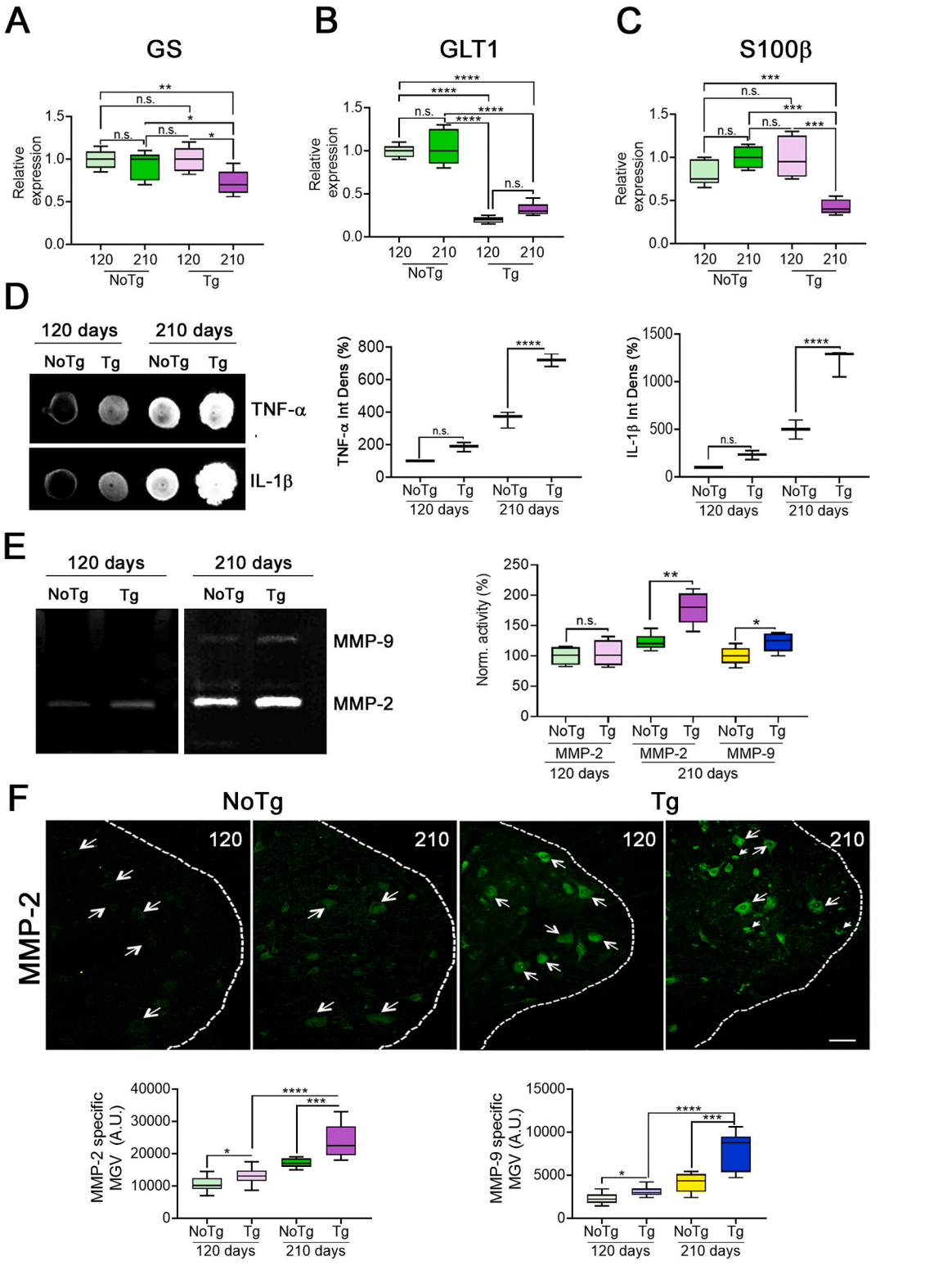

(caption on next page)

Fig. 4. Astrocyte markers and inflammatory cytokines in spinal cord samples. (A–C) Analysis of qPCR results evidencing statistically significant decreases in gene expression of GS (A), GLT1 (B) and S100β (C) in SC homogenates from Tg asymptomatic (120 day-old) and terminal (210 day-old) animals and age-matched NoTg brothers (5 replicates per animal sample, 7 animals). (D) Dot blot on the left showing the positive signals for TNF-α and IL-1β in SC homogenates from Tg asymptomatic (120 day-old) and terminal (210 day-old) animals and age-matched NoTg brothers. Charts on the right show the integrated density of each spot taking the values of 120 day-old NoTg rats as the controls. Each value was previously related to the integrated density of β-tubulin taken as the protein loading control. BSA was used as a negative control. Recombinant TNF-α was employed as the positive control (5 replicates per animal sample, 3 independent runs, 7 animals). (E) A gel zymogram showing white bands that evidence gelatin degradation due to MMP-9 and MMP-2 activities in SC samples from 120 day-old (left) and 210 day-old (right) NoTg and Tg rats. Note significant MMP-2 brighter signals in 210 day-old rats. Charts on the right show the quantitation of band areas and the statistical significance of differences among ages and NoTg and Tg samples. MMP-9 was not evaluated at 120 day-old because of the very low signal (5 replicates per animal sample, 3 independent runs, 7 animals). (F) Representative Z-stack confocal images of the ventral horn of lumbar SC of NoTg and Tg symptomatic rats immunostained against MMP-2. Note that positive cells are motor neurons of different sizes (larger ones pointed with long arrows and smaller ones pointed with short arrows) in sections from Tg animals. Dashed lines indicate the limit between gray and white matter highlighting that the signal is predominantly present in the gray matter. Calibration bars: 50 μm. Charts show that the MMPs′ signal intensity increased along disease progression suggesting that other cellular sources different from motor neurons that are dying and therefore diminishing its number, may be responsible for increased MMPs′ immunoreactivity along disease progression (~150 cells analyzed per replicate, 5 replicates per animal sample, 7 animals). In the charts A-C, values of SC samples of 120 day-old NoTg animals were represented in pale green and those of 120 day-old Tg animals in intense green; and SC samples from NoTg and Tg animals of 210 day-old were colored in pale and intense fuchsia, respectively. In the charts E and F, data from 120 and 210 day-old rats appear in pale and intense colors, respectively. MMP-2 results were represented in green and fuchsia for NoTg and Tg rats, whereas MMP-9 data from those animals appear in yellow and blue, respectively. Complete dot blots and zymograms of Fig. 4D and E are in Supplementary material. (For interpretation of the references to color in this figure legend, the reader is referred to the Web version of this article.)

● Preserved pharmacological resistance

Along culturing, AbAs did not show increased vulnerability to compounds that cause ~50 % of NoTg astrocyte death upon 24 h of treatment (Fig. 2D) [24,41–44], except upon Zn exposure (~↓ 25 %, $p = 0.0022$). Instead, significant increases were found after incubating HP vs. LP cultures with TN (~↑ 14 %, $p = 0.0022$); 300 μM 6AN (~↑ 10 %, $p = 0.0187$) and 10 μM FSK (~↑ 25 %, $p = 0.0069$), respectively. FSK was also employed [24,44] to check the existence of the typical stellate response that astrocytes suffer upon incubation with it without altering its survival [24]. Interestingly, LP and HP AbAs were vulnerable to violacein (Fig. 2E), a compound that inhibited glial reactivity and delayed neurodegeneration in the rat SOD1G93A model, likely by killing these cells among other beneficial effects [45]. Violacein employed concentrations did not affect the survival of primary cultured spinal astrocytes (AA) obtained from adult NoTg rats, but LP AbAs viability decreased once exposed to 150 (~↓ 27 %, $p < 0.0001$) and to 300 nmol/L (~↓ 52 %, $p < 0.0001$) violacein, respectively. HP AbAs viability was also affected by violacein but did not change at different concentrations (~↓ 50 % in both cases, $p = 0.8019$). Results also indicate a higher vulnerability of HP vs. LP AbAs ($p = 0.0002$) to 150 nmol/L violacein but not to 300 nmol/L ($p = 0.9910$).

● Diminished TNF-α and IL-lβ levels upon long lasting cultivation

The conditioned medium harvested from LP and HP AbAs cultured during 48 h in absence of FBS had significant levels of the pro-inflammatory cytokines TNF-α and IL-lβ. However, in LP AbAs both values were much higher than in HP cells (Fig. 3A). Quantitation of integrated density in dot blots containing the same amount of total proteins indicated that respective decreased values of both cytokines were (~↓ 22 %, $p = 0.0057$, $t = 5.408$, $df = 4$) and (~↓ 37 %, $p < 0.0001$, $t = 15.64$, $df = 4$) for TNF-α and IL-lβ in HP vs. LP cultures. No measurable levels of both cytokines were found in the conditioned medium from primary astrocytes.

● MMP-2 and MMP-9 decreased activities but raised immunoreactivity in HP vs. LP AbAs

Gelatin zymography showed lower signals in the conditioned medium of HP vs. LP AbAs, what was confirmed by the quantitative analysis that indicated less active MMP-2 (~↓ 37 %, $p < 0.0001$) and MMP-9 (~↓ 54 %, $p < 0.0001$) in HP cells (Fig. 3B). In contrast, the analysis of the immunoreactivity for both proteases indicated that MMP-2 net MGV from HP AbAs almost doubled that of LP (~↑ 45 %, $p = 0.0001$) whereas MGV of MMP-9 remained unchanged ($p = 0.8617$) (Fig. 3C), clearly suggesting that the synthesis of inactive MMP forms increases for MMP-2 and remain intact for MMP-9 during the long lasting cultivation.

3.2. Astrocyte and inflammation markers in the lumbar SC along disease progression

● GS, GLT1 and S100β gene expression studies

Analysis made in samples from 210 vs. 120 day-old animals revealed that NoTg rats preserved GS gene expression ($p > 0.9999$) but Tg decreased it significantly (~↓ 20 %, $p = 0.0372$). When comparing Tg with NoTg rats, GS gene expression was similar at the age of 120 day-old ($p = 0.4085$) but decreased at 210 day-old Tg samples (~↓ 30 %, $p = 0.0305$) (Fig. 4A). Differences among the whole group calculated with ordinary one-way ANOVA indicated statistical significance ($p = 0.0249$, $F = 4.084$).

Regarding GLT1 (Fig. 4B), evaluation of 210 vs. 120 day-old animals evidenced similar levels in NoTg ($p = 0.9315$) and Tg rats ($p =$

0.9840). The comparison of Tg with NoTg animals revealed less expression in Tg at 120 (~↓ 40 %, p = 0.0012) and at 210 day-old (~↓ 70 %, p < 0.0001). Ordinary one-way ANOVA for the whole group showed statistical significance (p value < 0.0001, F = 33.56).

Analysis of S100β gene expression (Fig. 4C) at 210 vs. 120 day-old showed similar values in NoTg (p = 0.3262) but significant decreases in Tg animals (~↓ 50 %, p = 0.0002). The comparison of Tg with NoTg samples indicated absence of differences at 120 day-old (p = 0.3262) but lower values in 210 day-old Tg respect to age-matched NoTg rats (~↓ 50 %, p = 0.0002). Ordinary one-way ANOVA for the whole group was p < 0.0001, F = 14.04.

- TNF-α and IL-lβ levels

As assessed in dot blots, homogenates from SC exhibited significant TNF-α levels and increased values when comparing samples from 210 vs. 120 day-old from NoTg (~↑ 200 %, p < 0.0001) or from Tg rats (~↑ 287 %, p < 0.0001). Comparison between age-matched Tg vs. NoTg animals revealed no differences at 120 day-old (p = 0.0652) but increased expression in Tg at 210 day-old (~↑ 110 %, p < 0.0001), respectively. Ordinary one-way ANOVA for the whole group showed significant differences (p < 0.0001, F = 185.3) (first chart, Fig. 4D).

Regarding IL-1β, increases in 210 vs. 120 day-old were found in NoTg (~↑ 250 %, p < 0.0001) and in Tg (~↑ 450 %, p < 0.0001) SC homogenates, respectively. Values were preserved when comparing Tg vs. NoTg samples at 120 day-old (~↑ 150 %, p = 0.077) but increased at 210 day-old (~↑ 200 %, p < 0.0001). Ordinary one-way ANOVA for the whole group showed significant differences (p < 0.0001, F = 91.67) (second chart, Fig. 4D).

- MMP-2 and MMP-9 raised activities along disease progression

Zymography analysis of MMP-2 activity in SC homogenates at both ages analyzed indicated preserved values in NoTg (p =

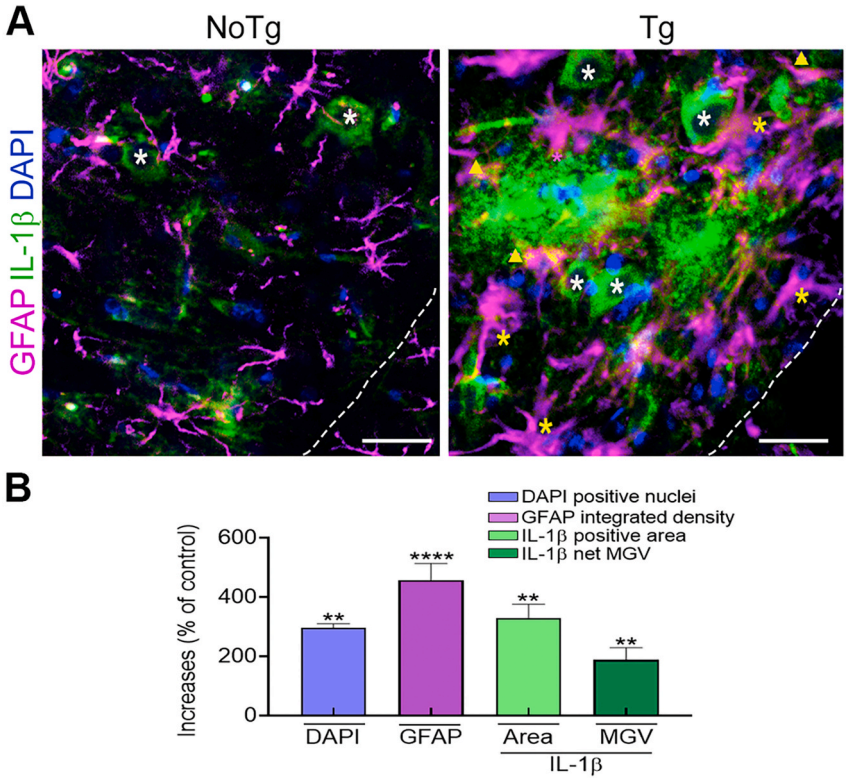

Fig. 5. IL-1β immunoreactivity in SC sections of 210 day-old animals. (A) Representative confocal Z-images of IL-1β (green) co-labeled with GFAP (fuchsia). Nuclei were labeled with DAPI. Note that IL-1β signal increased inside the soma of motor neurons (white asterisks) and as extra-neuronal signals in samples from Tg animals. Interestingly, IL-1β was expressed only in few reactive astrocytes that are seen in yellowish coloration (yellow triangles) but not in the majority of these cells in spite of the extensive astrogliosis evidenced by abundant cells with swollen bodies and thickened cell processes (fuchsia, yellow asterisks). The thin dashed white lines delimit the gray and white matter regions in the SC. Calibration bars: 30 μm. (B) Quantitation of main differences in SC sections of Tg vs. NoTg samples at 210 days (~150 cells analyzed per replicate, 5 replicates per animal sample, 7 animals). Values of each parameter in 210 day-old NoTg animals were taken as 100 %. Note significant increases in the DAPI (blue column) positive nucleus density; GFAP integrated density (fuchsia column) and IL-1β area and MGV (green columns), respectively. Levels of statistical significance were the same as the other figures. (For interpretation of the references to color in this figure legend, the reader is referred to the Web version of this article.)

0.03861) but increased in Tg (~↑ 76 %, p = 0.0003) samples, respectively. Augments were also found when comparing Tg vs. NoTg samples at 210 day-old (~↑ 47 %, p = 0.0026) but not at 120 day-old (p = 0.5348). Ordinary one-way ANOVA for the whole group showed significant differences (p = 0.0001, F = 15.40) (Fig. 4E). When analyzing MMP-9 in the same zymograms, non-quantifiable traces were found in 120 day-old NoTg and Tg animals but increased when comparing 210 day-old Tg vs. NoTg samples (~↑ 25 %, p = 0.0034). Statistical analysis using unpaired Student *t*-test showed t = 2.372 and df = 8 (Fig. 4E).

● Increased MMP-2 and -9 immunoreactivity in SC sections

Immunoreactivity against MMP-2 measured in spinal motor neurons (Fig. 4F) showed increases in 210 vs. 120 day-old in both NoTg (~↑ 60 %, p < 0.0001) and Tg samples (~↑ 82 %, p < 0.0001). Augments were also found when comparing Tg vs. NoTg samples at 120 day-old (~↑ 25 %, p = 0.015) and at 210 day-old (~↑ 40 %, p = 0.0004). Ordinary one-way ANOVA for the whole group showed significant differences (p < 0.0001, F = 91.67). When analyzing motor neuron MMP-9 immunoreactivity in the same SC sections, increases in 210 vs. 120 day-old were found in NoTg (~↑ 80 %, p < 0.0001) and in Tg (~↑ 150 %, p < 0.0001) samples, respectively. Higher values were also seen when comparing Tg vs. NoTg samples at 120 day-old (~↑ 38 %, p = 0.0394) and at 210 day-old (~↑ 88 %, p < 0.0001). Ordinary one-way ANOVA for the whole group showed significant differences (p < 0.0001, F = 74.09) (Fig. 4F), all indicating increased MMP-2 and MMP-9 activity and expression in symptomatic/terminal vs. asymptomatic Tg animals.

● Increased pro-inflammatory cytokines in SC sections of terminal Tg rats

IL-1β immunoreactivity was assessed in SC samples from terminal Tg animals and in their age-matched NoTg brothers. As Fig. 5A shows, in the SC section from NoTg animals there are few motor neurons with positive IL-1β signal and thin delicate GFAP positive astrocyte processes. Instead, the SC section from terminal Tg rats showed remaining motor neurons with brighter IL-1β signals and also its abundant presence in the gray matter outside but close to motor neurons. Interestingly, hypertrophic GFAP positive astrocytes were not enriched in IL-1β and only few of them showed a very low positive signal suggesting that other glial cells, probably microglia, could be the main sources of such inflammation mediator. Quantitation shown in Fig. 5B indicates increased cell density (~↑ 250 %, p = 0.009, t = 21.16, df = 20), GFAP integrated density (~↑ 400 %, p < 0.0001, t = 15.81, df = 25), and IL-1β positive areas (~↑ 300 %, p < 0.0001, t = 10.18, df = 24) and MGV (~↑ 210 %, p = 0.0011, t = 4.115, df = 14. All these values, strongly suggesting the co-existence of massive astrogliosis, likely with the presence of abundant AbAs, and inflammation.

In summary, results obtained in this work showed that along culturing, AbAs continued losing the expression of parameters critical to the maintenance of the CNS homeostasis. A similar tendency was found when comparing SC samples from symptomatic vs. asymptomatic Tg rats. Diminished values were also seen in AbAs inflammatory signaling and in MMP-2 and -9 activities in spite of a preserved immunoreactivity. Instead, SC samples increased inflammation markers and MMP-2 and MMP-9 gelatinase activities in the Tg symptomatic stage. Thus, only some AbAs' features seemed to be permanently acquired, while others might depend on the degenerating tissue from which they were isolated.

4. Discussion

4.1. Loss of homeostasis-related markers in HP vs. LP AbAs and in symptomatic vs. asymptomatic Tg animals

Glutamine synthase and GLT1 decreased gene expression and immunoreactivity was found in HP vs. LP AbAs as well as in the SC of symptomatic/terminal vs. asymptomatic Tg rats. As AbAs were cultured in basal conditions and without any injuring signaling, we can propose that there is a tendency to lack homeostatic parameters along culturing. This could be associated with increased proliferation that in turn could depend on decreased S100β levels [30] or of raising ER stress [61]. Thus, AbAs might progressively acquire properties of de-differentiated cells that lose lineage markers at expenses of increased proliferation [28].

Interestingly, a recent report [62] showed that serial passages caused that aged astrocyte phenotypes suffer progressive loss of homeostatic properties and increased senescence. Despite progressively loss of homeostatic properties, AbAs did not show replicative senescence [24,25] and continued increasing their proliferating rate along passages, confirming that these cells are not simply aged astrocytes. In addition, Ibarburu et al. [28] showed that HP AbAs also substantially preserved their neurotoxic capacity once transplanted to healthy wild type animals, indicating that AbAs maintained their ability to elicit glial reactivity and motor neuron ubiquitin aggregation, as well as their capacity to spread motor neuron damage along the neuroaxis [28]. In accordance, we have recently reported that AbAs emerge in the SC portion that innervates the earliest affected limbs and then propagates to the rest of the spinal cord spreading motor neuron damage and glial reactivity [29].

Respecting GLT1, our results showed decreased values in AbAs along culturing and in the SC tissue of Tg vs. NoTg rats. SC data found are in accordance with decreased GLT1 expression described in mice ALS SOD1 models [54] as well as in familial and sporadic ALS cases [8,30,63,64]. Statistically significant decreased gene and protein expression of GLT1 and GS are directly linked to lack of astrocyte homeostatic functions and protection against excitotoxicity, because decreased GLT1 impairs the astrocyte control of synaptic glutamate levels due to its minor uptake at the synaptic cleft [26,27,36]. Lack of GS also slows the conversion of glutamate to the glutamine that neurons will further employ during synaptic activity, then GS decreases impair proper glutamate synthesis and storage [38,65]. In addition, loss of GLT1 and GS impedes astrocyte ammonia clearance that is crucial to prevent neurotoxicity [36]. Furthermore, failure in the glutamate/glutamine cycle also affects the limiting step of the glutathione synthesis that in CNS is almost exclusively done by astrocytes [36], thus decreasing cellular antioxidant defenses. Then, as AbAs become the predominant glial

phenotype during disease progression [24,25,28,29], the GS and GLT1 decreases in SC of Tg rats might be attributed in part to the low content of both proteins in AbAs. If this could be the case, AbAs might be important contributors, likely determinants, of the homeostasis loss seen during the symptomatic up to the end stage of the disease.

Regarding S100β, it appears to integrate AbAs cytoskeletal elements [24,25], but there was decreased gene expression and immunoreactivity in HP vs. LP cells. This decrease could be associated with the cytoskeleton instability and exacerbated proliferative capacity [65] observed. S100β also deserves attention because it activates the nuclear factor NF-κB and downstream inflammatory signaling [39,40]. In this sense, decreased S100β values upon long lasting culture could be associated with the lower levels of inflammatory mediators found in HP vs. LP AbAs. Instead, in the SC sections, the previous report showed AbAs increase exponentially during disease progression and exhibited a more aggressive invading phenotype in symptomatic/terminal Tg animals. Thus, it might be probable that S100β levels in AbAs could predominantly affect cytoskeleton stability favoring its invasive properties as previously proposed [28,66].

4.2. AbAs phenotype was resistant to diverse pharmacological challenges except to violacein

Remarkably, in spite of the gene and protein expression changes found along culturing, LP and HP AbAs were equally resistant to the pharmacologic challenges employed at concentrations reported that affect astrocytes [15,25,41–44]. Our present findings are not contrary to previous reports that impeded AbAs emergence or their exponential increase [67,68], because we have obtained AbAs from Tg animals in their final stages and published therapies were applied before or just at the onset of the symptomatic stages [67,68]. Therefore, we propose that AbAs obtained from terminal animals are highly resistant to pharmacological modulation and could cope with significantly increased cellular stress as that produced by tunicamycin in spite of their own ER stress high basal levels. This behavior could seem part of the loss of typical features seen upon serial passaging as previously reported in normal astrocytes [61]. Strikingly, LP and HP AbAs were much more vulnerable to violacein than astrocytes obtained from NoTg animals. This effect seems to be associated to AbAs impaired cell proliferation and migration [29,45], although the underlying mechanisms are still under study.

4.3. Inflammatory profiles in AbAs vs. SC samples: a microenvironment-dependent signaling?

HP vs. LP AbAs significantly decreased inflammatory signaling as shown by descendent TNF-α and IL-1β levels and substantial diminished MMP-2 and -9 activities. These results appear similar to those described from serially passaged astrocytes [62] that showed loss of inflammatory signaling in particular of TNF-α and IL-1β expression. However, contrary to the senescent phenotype that these authors proposed, upon subsequent passages, AbAs do not show replicative senescence but increased cell proliferation. Then, AbAs only resembles part of the phenotype described in primary astrocytes [62], and their varying features could not only be attributed to passaging. Instead, we propose that AbAs inflammatory repertoire might depend on the microenvironment signaling. This hypothesis is highly supported by the fact that HP AbAs elicited neuronal damage and glial reactivity once injected in animals [28]. In this sense, preserved MMP-2 and -9 expressions in HP vs. LP cultures indicate that AbAs continue synthesizing these proteins and keep it in their inactive forms [58], allowing us to speculate that AbAs maintain their potential to immediately react to injuring conditions.

Regarding the data found in the SC samples, significant increases in TNF-α and IL-1β as well as in MMP-2 and -9 activities were seen in samples from Tg symptomatic/terminal vs. asymptomatic animals. Apart from participating in the neuroinflammatory response, TNF-α may inhibit glutamate transport on astrocytes [49], linking neuroinflammation to excitotoxicity. This role of TNF-α seems particularly important in the ALS model used because it could partly explain the decrease in GLT-1. Therefore, the coexistence of elevated TNF-α levels and the decreases in GLT1 and GS aggravate the two main pathological mechanisms that occur in ALS and could explain, at least in part, the aggressiveness of the model. On the other hand, IL-1β is proposed as one of the initiating signals in ALS [48], and then increased levels may help to widespread damaging cascades along the SC.

Our results show that MMP-2 and MMP-9 activities in symptomatic/terminal Tg rats increased when compared to asymptomatic rats, likely due to the increasing inflammatory signaling associated to damage progression [11,12,32]. Increased MMP-2 and -9 activities are higher that augments in the immunoreactivity, and could be attributed, at least initially, to the enhanced processing of inactive forms instead of newly synthesized proteins as previously reported [59]. However, absolute MMP-2 and -9 activities found in rat SC homogenates seem low when compared to values reported in SOD1G93A mice [32,62]. We attribute these differences to the much slower disease progression in rats than in mice [12,32,34], and in part to the more extended lifespan of our colony related to the initial reports [8]. In both cases, MMP-2 and -9 activities seem directly associated with the time course of the disease, either as consequences or as causing agents, as proposed by Hannocks et al. [35].

In line with this idea, in pathological conditions, MMP-2 and -9 may contribute to neuroinflammation by directly activating inflammatory candidates such as by processing membrane-bound isoforms into soluble active forms [33] or indirectly by acting on enzymes which substrates are inflammatory signaling molecules [33,34]). In turn, MMP-2 and -9 may also play as neuroinflammatory signals per se because both are able to trigger glial activation and further secretion of pro-inflammatory cytokines [33,34,48]. Furthermore, these pro-inflammatory cytokines, such as TNF-α does, may stimulate MMP-2 and -9 transcription reinforcing neuroinflammation through an auto-amplifying deleterious loop [49]. In accordance, MMP-2 and IL-1β in the SC showed high signals in motor neurons that are the cells likely injured and prone to die, probably indicating that these cells seem to be the preferred targets of the deleterious actions of both proteins. High extracellular expression of these proteins also indicates significant secretion from yet unidentified cellular sources. Due to the low IL-1β levels found in GFAP positive astrocytes, both results strongly suggest that microglial cells are involved in those augments, therefore it must be studied due to its described roles in the synthesis and release of pro-inflammatory markers [60,70].

4.4. AbAs signaling may contribute to reinforcing degenerating microenvironment and their own phenotype

Here we have shown that AbAs in culture recapitulate many features of what is occurring during disease progression, mostly those related to continuous loss of homeostatic functions as well as increased cell proliferation and ER stress suggesting the existence of a powerful but yet unknown autocrine signaling. Instead, upon long lasting culture, the characteristics related to inflammation decayed, suggesting a dependence on environmental signaling as often described in astrocytes [2,18,46,47,62]. Recent data show that astrocytes are gaining importance in CNS intercellular signaling because they can detect their own activity and those of surrounding cells, or feedback or initiate cellular communication on their own [26,27]. Astrocytes play these roles often through a highly enriched gliocrine system that is much slower than the synaptic system but lasts longer and can modulate broader fields [26,27]. Our previous results show that AbAs exhibit a plethora of signals evidencing their mutual communication as well as strong interchanging activity with the extracellular medium likely through multiple vesicles that are different in size, shedding and content, but also associated to exocytosis or endocytosis, suggesting different ways of intercellular communication [25].

Astrocyte gliocrine system is altered in disease and contributes to the development of neurodegeneration [26,27]. Ultrastructural analysis showed that AbAs possess multiple signs of altered gliocrine system as suggested by the presence of multiple multivesicular and multi-membrane bodies as well as abundance of intracellular inclusions [25]. AbAs are also extremely enriched in stress granules [25] that were formed in response to various stresses present in the degenerating microenvironment and likely contribute to their metabolic reprogramming and survival [25]. In addition, aberrant responses to stress may contribute to the generation of pathological persistent stress granules that could be implicated in neurodegenerative diseases [69]. This may allow us to suggest that by these means, AbAs not only contribute to the massive motor neuron death, but also to the maintenance and reinforcement of their own phenotype. Thus, knowing AbAs is necessary to cut this auto-reinforced disrupting loop not only to avoid the perpetuation of these unprecedented toxic cells but also to impair its autocrine and paracrine signaling.

5. Conclusion

Overall, our results show that AbAs constitute a particular phenotype that resembles some of the aspects of ALS disease progression in the SOD1G93A rat model, suggesting that many of the properties acquired during AbAs emergence are permanent. Instead, the characteristics related to inflammation may strongly depend on the microenvironment signaling. In addition, the failure of pharmacological modulation suggests that AbAs have potent survival mechanisms. This not only will impair trophic support but also widespread sustained failures in CNS homeostasis and potentiate damaging signals, both favoring the emergence and proliferation of toxic phenotypes such AbAs.

Funding statement

This research was partially funded by IIBCE (MEC-Uruguay), PEDECIBA and ANII (Graduate scholarships for G.O. and E.I).

Institutional review board statement

The local Ethics Committee approved the experimental procedures (CEUA-IIBCE, MEC, Uruguay, protocol number: 004/09/2015).

Informed consent statement

Not applicable.

Data availability statement

The data presented in this study are available on reasonable request to the corresponding author.

CRediT authorship contribution statement

Gabriel Otero: Writing – original draft, Visualization, Software, Methodology, Investigation, Formal analysis, Data curation, Conceptualization. **Carmen Bolatto:** Writing – review & editing, Writing – original draft, Visualization, Supervision, Software, Methodology, Investigation, Funding acquisition, Formal analysis, Conceptualization. **Eugenia Isasi:** Writing – review & editing, Writing – original draft, Visualization, Software, Methodology, Investigation, Funding acquisition. **Sofía Cerri:** Writing – original draft, Visualization, Validation, Software, Methodology, Investigation, Formal analysis. **Paola Rodríguez:** Writing – original draft, Visualization, Validation, Software, Methodology, Investigation, Formal analysis. **Daniela Boragno:** Writing – original draft, Validation, Software, Methodology, Investigation, Formal analysis. **Marta Marco:** Writing – review & editing, Writing – original draft, Validation, Methodology, Conceptualization. **Cristina Parada:** Writing – review & editing, Writing – original draft, Visualization, Validation, Software, Methodology, Investigation, Formal analysis. **Matías Stancov:** Writing – original draft, Validation, Software, Methodology, Investigation, Formal analysis. **María Noel Cuitinho:** Writing – original draft, Validation, Software, Methodology, Investigation, Formal analysis. **Silvia Olivera-Bravo:** Writing – review & editing, Writing – original draft, Visualization, Validation, Supervision, Software, Resources, Project administration, Methodology, Investigation, Funding acquisition, Formal analysis, Data

curation, Conceptualization.

Declaration of competing interest

The authors declare the following financial interests/personal relationships which may be considered as potential competing interests: Silvia Olivera-Bravo reports financial support was provided by Institute for Biological Research Clemente Estable.Silvia Olivera-Bravo reports equipment, drugs, or supplies was provided by Programme for the Development of Basic Sciences. Gabriel Otero, Eugenia Isasi reports financial support was provided by National Agency for Research and Innovation. If there are other authors, they declare that they have no known competing financial interests or personal relationships that could have appeared to influence the work reported in this paper.

Acknowledgments

We thank Dr. Freddy Ibañez-Carrasco for the academic support. We also thank the staff of the IIBCE animal house and technical platforms.

Appendix A. Supplementary data

Supplementary data to this article can be found online at https://doi.org/10.1016/j.heliyon.2024.e30360.

References

[1] D.W. Cleveland, J.D. Rothstein, From Charcot to Lou Gehrig: deciphering selective motor neuron death in ALS, Nat. Rev. Neurosci. 2 (11) (2001) 806–819.
[2] K. Yamanaka, O. Komine, The multi-dimensional roles of astrocytes in ALS, Neurosci. Res. 126 (2018) 31–38.
[3] A. Al-Chalabi, F. Fang, M.F. Hanby, P.N. Leigh, C.E. Shaw, W. Ye, F.J. Rijsdijk, An estimate of amyotrophic lateral sclerosis heritability using twin data, J. Neurol. Neurosurg. Psychiatry 81 (12) (2010) 1324–1326.
[4] M.E. Cudkowicz, L. Warren, J.W. Francis, K.J. Lloyd, R.M. Friedlander, L.F. Borges, N. Kassem, T.L. Munsat, R.H. Brown Jr., Intrathecal administration of recombinant human superoxide dismutase 1 in amyotrophic lateral sclerosis: a preliminary safety and pharmacokinetic study, Neurol. 49 (1997) 213–222.
[5] D.R. Rosen, T. Siddique, D. Patterson, D.A. Figlewicz, P. Sapp, A. Hentati, D. Donaldson, J. Goto, J.P. O'Regan, H.X. Deng, et al., Mutations in Cu/Zn superoxide dismutase gene are associated with familial amyotrophic lateral sclerosis, Nature 362 (6415) (1993) 59–62.
[6] S. Boillée, C. Vande Velde, D.W. Cleveland, ALS: a disease of motor neurons and their non neuronal neighbors, Neuron 52 (2006) 39–59.
[7] M.E. Gurney, H. Pu, A.Y. Chiu, M.C. Dal Canto, C.Y. Polchow, D.D. Alexander, J. Caliendo, A. Hentati, Y.W. Kwon, H.X. Deng, Motor neuron degeneration in mice that express a human Cu,Zn superoxide dismutase mutation, Science 264 (1994) 1772–1775.
[8] D.S. Howland, J. Liu, Y. She, B. Goad, N.J. Maragakis, B. Kim, J. Erickson, J. Kulik, L. DeVito, G. Psaltis, L.J. De Gennaro, D.W. Cleveland, J.D. Rothstein, Focal loss of the glutamate transporter EAAT2 in a transgenic rat model of SOD1 mutant-mediated amyotrophic lateral sclerosis (ALS), Proc. Natl. Acad. Sci. U.S.A. 99 (2002) 1604–1609.
[9] B.J. Turner, K. Transgenics Talbot, Toxicity and therapeutics in rodent models of mutant SOD1 mediated familial ALS, Prog. Neurobiol. 85 (2008) 4–134.
[10] D. Jaarsma, E. Teuling, E.D. Haasdijk, C.I. De Zeeuw, C.C. Hoogenraad, Neuron-specific expression of mutant superoxide dismutase is sufficient to induce amyotrophic lateral sclerosis in transgenic mice, J. Neurosci. 28 (9) (2008) 2075–2088.
[11] H. Ilieva, M. Polymenidou, D.W. Cleveland, Non–cell autonomous toxicity in neurodegenerative disorders: ALS and beyond, J. Cell Biol. 187 (2009) 761–772.
[12] T. Philips, J.D. Rothstein, Rodent models of amyotrophic lateral sclerosis, Curr. Protoc. Pharmacol. 69 (5) (2015), 67.1-5.67.21.
[13] M. Izrael, S.G. Slutsky, M. Revel, Rising stars: astrocytes as a therapeutic target for ALS disease, Front. Neurosci. 14 (2020) 824.
[14] C. Hetz, P. Thielen, S. Matus, M. Nassif, F. Court, R. Kiffin, G. Martinez, A.M. Cuervo, R.H. Brown, L.H. Glimcher, XBP-1 deficiency in the nervous system protects against amyotrophic lateral sclerosis by increasing autophagy, Genes Dev. 23 (2009) 2294–2306.
[15] V. Valenzuela, M. Oñate, C. Hetz, F.A. Court, Injury to the nervous system: a look into the ER, Brain Res. 1648 (2016) 617–625.
[16] H. Kawamata, G. Manfredi, Mitochondrial dysfunction and intracellular calcium dysregulation in ALS, Mech. Ageing Dev. 131 (2010) 517–526.
[17] D. Trotti, M. Aoki, P. Pasinelli, U.V. Berger, N.C. Danbolt, R.H. Brown Jr., M.A. Hediger, Amyotrophic lateral sclerosis-linked glutamate transporter mutant has impaired glutamate clearance capacity, J. Biol. Chem. 276 (1) (2001) 576–582.
[18] M. Nagai, D.B. Re, T. Nagata, A. Chalazonitis, T.M. Jessell, H. Wichterle, S. Przedborski, Astrocytes expressing ALS-linked mutated SOD1 release factors selectively toxic to motor neurons, Nat. Neurosci. 10 (2007) 615–622.
[19] P. Cassina, A. Cassina, M. Pehar, R. Castellanos, M. Gandelman, A. de León, K.M. Robinson, R.P. Mason, J.S. Beckman, L. Barbeito, R. Radi, Mitochondrial dysfunction in SOD1G93A-bearing astrocytes promotes motor neuron degeneration: prevention by mitochondrial-targeted antioxidants, J. Neurosci. 28 (2008) 4115–4122.
[20] F.P. Di Giorgio, G.L. Boulting, S. Bobrowicz, K.C. Eggan, Human embryonic stem cell-derived motor neurons are sensitive to the toxic effect of glial cells carrying an ALS-causing mutation, Cell Stem Cell 3 (2008) 637–648.
[21] A.M. Haidet-Phillips, M.E. Hester, C.J. Miranda, K. Meyer, L. Braun, A. Frakes, S. Song, S. Likhite, M.J. Murtha, K.D. Foust, M. Rao, A. Eagle, A. Kammesheidt, A. Christensen, J.R. Mendell, A.H. Burghes, B.K. Kaspar, Astrocytes from familial and sporadic ALS patients are toxic to motor neurons, Nat. Biotechnol. 29 (2011) 824–828.
[22] D.B. Re, V. Le Verche, C. Yu, M.W. Amoroso, K.A. Politi, S. Phani, B. Ikiz, L. Hoffmann, M. Koolen, T. Nagata, D. Papadimitriou, P. Nagy, H. Mitsumoto, S. Kariva, H. Wichterle, C.E. Henderson, S. Przedborski, Necroptosis drives motor neuron death in models of both sporadic and familial ALS, Neuron 81 (2014) 1001–1008.
[23] A. Birger, I. Ben-Dor, M. Ottolenghi, T. Turetsky, Y. Gil, S. Sweetat, L. Perez, V. Belzer, N. Casden, D. Steiner, M. Izrael, E. Galun, E. Feldman, O. Behar, B. Reubinoff, Human iPSC-derived astrocytes from ALS patients with mutated C9ORF72 show increased oxidative stress and neurotoxicity, EBioMedicine 50 (2019) 274–289.
[24] P. Diaz-Amarilla, S. Olivera-Bravo, E. Trias, A. Cragnolini, L. Martínez-Palma, P. Cassina, J. Beckman, L. Barbeito, Phenotypically aberrant astrocytes that promote motoneuron damage in a model of inherited amyotrophic lateral sclerosis, Proc. Natl. Acad. Sci. U.S.A. 108 (2011) 18126–18131.
[25] M. Jimenez-Riani, P. Diaz-Amarilla, E. Isasi, G. Casanova, L. Barbeito, S. Olivera-Bravo, Ultrastructural features of aberrant glial cells isolated from the spinal cord of paralytic rats expressing the amyotrophic lateral sclerosis-linked SOD1G93A mutation, Cell Tissue Res. 370 (3) (2017) 391–401.
[26] R. Zorec, V. Parpura, A. Verkhratsky, Astroglial vesicular trafficking in neurodegenerative diseases, Neurochem. Res. 42 (3) (2017) 905–917.
[27] N. Vardjan, V. Parpura, A. Verkhratsky, R. Zorec, Gliocrine system: astroglia as secretory sells of the CNS, Adv. Exp. Med. Biol. 1175 (2019) 93–115.

[28] S. Ibarburu, E. Trias, N. Lago, H. Peluffo, R. Barreto-Núñez, V. Varela, J.S. Beckman, L. Barbeito, Focal transplantation of aberrant glial cells carrying the SOD1G93A mutation into rat spinal cord induces extensive gliosis, Neuroimmunomodulation 24 (3) (2017) 143–153.
[29] G. Otero, C. Parada, P. Díaz-Amarilla, E. Isasi, C. Bolatto, S. Olivera-Bravo, Contribution of aberrant astrocytes to motor neuron damage and death in the SOD1G93A rat experimental model of ALS, in: L.F. Ibañez-Valdés, W. Sisulu (Eds.), Novel Aspects on Motor Neuron Disease, vol. 1, IntechOpen, London, UK, 2019, pp. 1–11.
[30] J.D. Rothstein, M. Van Kammen, A.I. Levey, L.J. Martin, R.W. Kuncl, Selective loss of glial glutamate transporter GLT-1 in amyotrophic lateral sclerosis, Ann. Neurol. 38 (1) (1995) 73–84.
[31] J.D. Rothstein, M. Dykes-Hoberg, C.A. Pardo, L.A. Bristol, L. Jin, R.W. Kuncl, Y. Kanai, M.A. Hediger, Y. Wang, J.P. Schielke, D.F. Welty, Knockout of glutamate transporters reveals a major role for astroglial transport in excitotoxicity and clearance of glutamate, Neuron 16 (3) (1996) 675–686.
[32] L. Fang, M. Teuchert, F. Huber-Abel, D. Schattauer, C. Hendrich, J. Dorst, H. Zettlmeissel, M. Wlaschek, K. Scharffetter-Kochanek, T. Kapfer, H. Tumani, A. C. Ludolph, J. Brettschneider, MMP-2 and MMP-9 are elevated in spinal cord and skin in a mouse model of ALS, J. Neurol. Sci. 294 (1–2) (2010) 51–56.
[33] A. Kaplan, K.J. Spiller, C. Towne, K.C. Kanning, G.T. Choe, A. Geber, T. Akay, P. Aebischer, C.E. Henderson, Neuronal matrix metalloproteinase-9 is a determinant of selective neurodegeneration, Neuron 81 (2) (2014) 333–348.
[34] M. Łukaszewicz-Zając, B. Mroczko, A. Słowik, Matrix metalloproteinases (MMPs) and their tissue inhibitors (TIMPs) in amyotrophic lateral sclerosis (ALS), J. Neural. Transm. 121 (11) (2014) 387–397.
[35] M.J. Hannocks, X. Zhang, H. Gerwien, A. Chashchina, M. Burmeister, E. Korpos, J. Song, L. Sorokin, The gelatinases, MMP-2 and MMP-9, as fine tuners of neuroinflammatory processes, Matrix Biol. 75–76 (2019) 102–113.
[36] N.J. Maragakis, J.D. Rothstein, Mechanisms of Disease: astrocytes in neurodegenerative disease, Nat. Clin. Pract. Neurol. 2 (12) (2006) 679–689.
[37] A. Verkhratsky, V. Parpura, N. Vardjan, R. Zorec, Physiology of astroglia, Adv. Exp. Med. Biol. 1175 (2019) 45–91.
[38] A.R. Jayakumar, M.D. Norenberg, Glutamine synthetase: role in neurological disorders, Adv. Neurobiol. 13 (2016) 327–350.
[39] R. Donato, G. Sorci, F. Riuzzi, C. Arcuri, R. Bianchi, F. Brozzi, C. Tubaro, I. Giambanco, S100B's double life: intracellular regulator and extracellular signal, Biochim. Biophys. Acta 1793 (6) (2009) 1008–1022.
[40] R.E. Gonzalez-Reyes, M.G. Rubiano, Astrocyte's RAGE: more than just a question of mood, Cent. Nerv. Syst. Agents Med. Chem. 18 (1) (2018) 39–48.
[41] R.L. Tyson, J. Perron, G.R. Sutherland, 6-Aminonicotinamide inhibition of the pentose phosphate pathway in rat neocortex, Neuroreport 11 (9) (2000) 1845–1848.
[42] G.M. Bishop, R. Dringen, S.R. Robinson, Zinc stimulates the production of toxic reactive oxygen species (ROS) and inhibits glutathione reductase in astrocytes, Free Rad. Biol. Med. 42 (8) (2007) 1222–1230.
[43] L. Cheng, H. Zhao, W. Zhang, B. Liu, Y. Liu, Y. Guo, L. Nie, Overexpression of conserved dopamine neurotrophic factor (CDNF) in astrocytes alleviates endoplasmic reticulum stress-induced cell damage and inflammatory cytokine secretion, Biochem. Biophys. Res. Comm. 435 (1) (2013) 34–39.
[44] K. Ravnskjaer, A. Madiraju, M. Montminy, Role of the cAMP pathway in glucose and lipid metabolism, Handbook Exp. Pharmacol. 233 (2016) 9–49.
[45] S. Olivera-Bravo, C. Bolatto, G. Otero Damianovich, M. Stancov, S. Cerri, P. Rodríguez, D. Boragno, K. Hernández Mir, M.N. Cuitiño, F. Larrambembere, E. Isasi, D. Alem, L. Canclini, M. Marco, D. Davyt, P. Díaz-Amarilla, Neuroprotective effects of violacein in a model of inherited amyotrophic lateral sclerosis, Sci. Rep. 12 (1) (2022) 4439.
[46] E. Colombo, C. Farina, Astrocytes: key regulators of neuroinflammation, Trends Immunol. 37 (9) (2016) 608–620.
[47] M. Neal, J.R. Richardson, Epigenetic regulation of astrocyte function in neuroinflammation and neurodegeneration, Biochim. Biophys. Acta, Mol. Basis Dis. 1864 (2) (2018) 432–443.
[48] F. Meissner, K. Molawi, A. Zychlinsky, Mutant superoxide dismutase 1-induced IL-1beta accelerates ALS pathogenesis, Proc. Natl. Acad. Sci. U. S. A. 107 (29) (2010) 13046–13050.
[49] G. Olmos, J. Llado, Tumor necrosis factor alpha: a link between neuroinflammation and excitotoxicity, Mediators Inflamm 2014 (2014) 861231.
[50] M.R. Vargas, M. Pehar, P. Cassina, J.S. Beckman, L. Barbeito, Increased glutathione biosynthesis by Nrf2 activation in astrocytes prevents p75NTR-dependent motor neuron apoptosis, J. Neurochem. 97 (3) (2006) 687–696.
[51] E. Isasi, N. Korte, V. Abudara, D. Attwell, S. Olivera-Bravo, Glutaric acid affects pericyte contractility and migration: possible implications for GA-I pathogenesis, Mol. Neurobiol. 56 (11) (2019) 7694–7707.
[52] S. Olivera, A. Fernandez, A. Latini, J.C. Rosillo, G. Casanova, M. Wajner, P. Cassina, L. Barbeito, Astrocytic proliferation and mitochondrial dysfunction induced by accumulated glutaric acidemia I (GAI) metabolites: possible implications for GAI pathogenesis, Neurobiol. Dis. 32 (3) (2008) 528–534.
[53] P. Skehan, R. Storeng, D. Scudiero, A. Monks, J. McMahon, D. Vistica, J.T. Warren, H. Bokesch, S. Kenney, M.R. Boyd, New colorimetric cytotoxicity assay for anticancer-drug screening, J. Natl. Cancer Inst. 82 (13) (1990) 1107–1112.
[54] T. Mosmann, Rapid colorimetric assay for cellular growth and survival: application to proliferation and cytotoxicity assays, J. Immunol. Meth. 65 (1–2) (1983) 55–63.
[55] E. Isasi, L. Barbeito, S. Olivera-Bravo, Increased blood-brain barrier permeability and alterations in perivascular astrocytes and pericytes induced by intracisternal glutaric acid, Fluids Barriers CNS 11 (2014) 15.
[56] K.J. Livak, T.D. Schmittgen, Analysis of relative gene expression data using real-time quantitative PCR and the 2(-Delta DeltaC(T)), Methods 25 (4) (2001) 402–408.
[57] S.M. Borghi, V. Fattori, F.A. Pinho-Ribeiro, T.P. Domiciano, M.M. Miranda-Sapla, T.H. Zaninelli, R. Casagrande, P. Pinge-Filho, W.R. Pavanelli, J.C. Alves-Filho, F.Q. Cunha, T.M. Cunha, W.A. Verri, Contribution of spinal cord glial cells to L. amazonensis experimental infection-induced pain in BALB/c mice, J. Neuroinflam. 16 (2019) 113.
[58] G.M. Palomo, V. Granatiero, H. Kawamata, C. Konrad, M. Kim, A.J. Arreguin, D. Zhao, T.A. Milner, G. Manfredi, Parkin is a disease modifier in the mutant SOD1 mouse model of ALS, EMBO Mol. Med. 10 (10) (2018).
[59] M. Marco, D. Boragno, P. Rodríguez, V. Mestre Cordero, N. Pereira, P. Berasain, F. Cadenas, C. Rodríguez, A. Moreira, X. Simoff, V. Bianchi, A. Barindelli, P. Fielitz, S. Olivera-Bravo, Gelatinases as markers of chronic alcohol consumption: a pilot study in Uruguay, Anales De La Facultad De Medicina, Universidad De La República, Uruguay 7 (1) (2020) e2020v7n1a3.
[60] E. Trias, P. Diaz-Amarilla, S. Olivera-Bravo, E. Isasi, D.A. Drechsel, N. Lopez, C.S. Bradford, K.E. Ireton, J.S. Beckman, L. Barbeito, Phenotypic transition of microglia into astrocyte-like cells associated with disease onset in a model of inherited ALS, Front. Cell. Neurosci. 24 (7) (2013) 274.
[61] S. Luo, C. Mao, B. Lee, A.S. Lee, GRP78/BiP is required for cell proliferation and protecting the inner cell mass from apoptosis during early mouse embryonic development, Mol. Cell Biol. 26 (15) (2006) 5688–5697.
[62] M. Bang, E.L. Gonzales, C.Y. Shin, K.J. Kwon, Late passage cultivation induces aged astrocyte phenotypes in rat primary cultured cells, Biomol Ther (Seoul). 29 (2) (2021) 144–153.
[63] L.I. Bruijn, M.W. Becher, M.K. Lee, K.L. Anderson, N.A. Jenkins, N.G. Copeland, S.S. Sisodia, J.D. Rothstein, D.R. Borchelt, D.L. Price, D.W. Cleveland, ALS-linked SOD1 mutant G85R mediates damage to astrocytes and promotes rapidly progressive disease with SOD1-containing inclusions, Neuron 18 (2) (1997) 327–338.
[64] H. Guo, L. Lai, M.E. Butchbach, M.P. Stockinger, X. Shan, G.A. Bishop, C.L. Lin, Increased expression of the glial glutamate transporter EAAT2 modulates excitotoxicity and delays the onset but not the outcome of ALS in mice, Hum. Mol. Genet. 12 (19) (2003) 2519–2532.
[65] C.F. Rose, A. Verkhratsky, V. Parpura, Astrocyte glutamine synthetase: pivotal in health and disease, Biochem. Soc. Trans. 41 (6) (2013) 1518–1524.
[66] C.M. Fife, J.A. McCarroll, M. Kavallaris, Movers and shakers: cell cytoskeleton in cancer metastasis, Br. J. Pharmacol. 171 (24) (2014) 5507–5523.
[67] L. Martinez-Palma, E. Miquel, V. Lagos-Rodriguez, L. Barbeito, A. Cassina, P. Cassina, Mitochondrial modulation by dichloroacetate reduces toxicity of aberrant glial cells and gliosis in the SOD1G93A rat model of amyotrophic lateral sclerosis, Neurotherapeutics 16 (1) (2019) 203–215.

[68] E. Trias, S. Ibarburu, R. Barreto-Núñez, J. Babdor, T.T. Maciel, M. Guillo, L. Gros, P. Dubreuil, P. Díaz-Amarilla, P. Cassina, L. Martinez-Palma, I.C. Moura, J. S. Beckman, O. Hermine, L. Barbeito, Post-paralysis tyrosine kinase inhibition with masitinib abrogates neuroinflammation and slows disease progression in inherited amyotrophic lateral sclerosis, J. Neuroinflam. 13 (1) (2016) 177.
[69] V.M. Advani, P. Ivanov, Stress granule subtypes: an emerging link to neurodegeneration, Cell. Mol. Life Sci. (23) (2020) 4827–4845.
[70] J.A. Smith, A. Das, S.K. Ray, N.L. Banik, Role of pro-inflammatory cytokines released from microglia in neurodegenerative diseases, Brain Res. Bull. 87 (1) (2012) 10–20.